Catalysis Science & Technology

# New findings and current controversies in the reaction of ruthenium red and ammonium cerium(IV) nitrate: Focus on the precipitated compound

| | |
|---|---|
| Journal: | *Catalysis Science & Technology* |
| Manuscript ID | CY-ART-12-2019-002499.R1 |
| Article Type: | Paper |
| Date Submitted by the Author: | 26-Feb-2020 |
| Complete List of Authors: | Sarvi, Bahram; Institute for Advanced Studies in Basic Sciences (IASBS), Chemistry<br>Hosseini, Seyedeh Maedeh; Institute for Advanced Studies in Basic Sciences<br>Deljoo, Bahareh ; Institute of Materials Science, University of Connecticut, Storrs, CT 06269, USA<br>El-Sawy, Abdelhamid ; Tanta University<br>Shirazi Amin, Alireza ; University of Connecticut, 55 North Eagleville Road, Unit 3060 Storrs, CT 06269-3060, USA, Department of Chemistry<br>Aindow, Mark; University of Connecticut, Materials Science and Engineering<br>Suib, Steven; University of Connecticut, U-60, Department of Chemistry<br>Najafpour, Mohammad; Institute for Advanced Studies in Basic Sciences (IASBS), Chemistry |
| | |

# New findings and current controversies in the reaction of ruthenium red and ammonium cerium(IV) nitrate: Focus on the precipitated compound

Bahram Sarvi,[a] Seyed Maedeh Hosseini,[a] Bahareh Deljoo,[b,c] Abdelhamid El-Sawy,[d] Alireza Shirazi Amin,[e] Mark Aindow[b,c], Steven L. Suib,[e,b,c*] and Mohammad Mahdi Najafpour[a,f,g*]

a. Department of Chemistry, Institute for Advanced Studies in Basic Science (IASBS), Zanjan, 45137-66731, Iran
b. Institute of Materials Science, University of Connecticut, 97 North Eagleville Road, Storrs, CT, 06269-3136, USA
c. Department of Materials Science and Engineering, University of Connecticut, 97 North Eagleville Road, Storrs, CT, 06269-3136, USA
d. Department of Chemistry, Faculty of Science, Tanta University, 31527, Tanta, Egypt
e. Department of Chemistry, University of Connecticut, 55 North Eagleville Road, Unit 3060, Storrs, CT, 06269-3060, USA
f. Center of Climate Change and Global Warming, Institute for Advanced Studies in Basic Science (IASBS), Zanjan, 45137-66731, Iran
g. Research Center for Basic Sciences & Modern Technologies (RBST), Institute for Advanced Studies in Basic Sciences (IASBS), Zanjan 45137-66731, Iran

*Corresponding Authors: steven.suib@uconn.edu (SS); mmnajafpour@iasbs.ac.ir (MMN).

**Abstract**

Finding the true catalyst has always been a challenging step toward the exploration, underestanding, and design of catalytic systems for water-oxidation reaction. Many homogeneous and heterogeneous transition metal complexes have been reported that can undergo a complete transformation to the true catalysts during water-oxidation reaction. Herein, the transformation of the previously-explored rethenium red ($[(NH_3)_5RuORu(NH_3)_4ORu(NH_3)_5]Cl_6$) catalyst in the presence of ammonium cerium(IV) nitrate is reported. For the first time, it is reported that a heterogeneous nano-sized ruthenium-cerium compound is formed by the electrostatic interaction of $[(NH_3)_5RuORu(NH_3)_4ORu(NH_3)_5]$,$^{6+/7+}$ nitrate ions, and the products of the reduction of ammonium cerium(IV) nitrate.

**Introduction**

Finding an efficient and stable water-oxidizing catalyst is a crucial step in water splitting that leads to a less expensive and more efficient way to store solar energy in the form of hydrogen.[1-5] The stored hydrogen can be used as a green fuel when other sources are not readily accessible. Thus, water-oxidation reaction (WOR), which provides electrons for proton reduction at low cost, will be an essential reaction as we seek to change our source of energy from fossil fuels to a sustainable and clean alternative.[1-5] Many transition metal compounds have been established as promising catalysts for WOR.[6-9] Among these compounds, many ruthenium complexes have been studied extensively as promising homogeneous catalysts for WOR by Meyer, Hurst, Sun, Llobet and other research groups.[10-27] Surprising, some of these ruthenium complexes can oxidize water three times more efficiently than the biological water-oxidizing complex in Photosystem II.[18,19] Meyer and co-workers were the first to report $[(bpy)_2(OH_2)RuORu(OH_2)(bpy)_2]^{4+}$, known as the "blue dimer", as a water-oxidizing catalyst which made a significant contribution to this field.[20] Then, Kaneko[21] and Meyer[22] reported that $[(NH_3)_5RuORu(NH_3)_4ORu(NH_3)_5]Cl_6$ (known as ruthenium red (RuR)) and its analogs are efficient molecular catalysts for WOR. However, questions remain about the character of the true catalyst and about the mechanism that is involved in WORs catalyzed by RuR. As discussed by the Llobet's group, no $RuO_2$ was detected when ruthenium complexes with stable ligands applied as the water-oxidizing catalyst.[27] Whereas, the formation of $RuO_2.xH_2O$ in the form of a black precipitate and the subsequent deactivation of the catalyst were observed when ruthenium complexes bearing easily oxidized ligands such as benzylic-, pyridylbenzyllic-, or amine-type groups had been used.[27] Having readily oxidizable ligands, RuR is also prone to transformation, and this phenomenon hinders the simplicity of the study of water-oxidation mechanism and finding the true catalyst. Russel *et al*. provided evidence that a mixture of RuR as a homogeneous water-oxidizing precatalyst, in the presence of ammonium cerium(IV) nitrate

(CAN), was irreversibly decomposed to obtain a ruthenium complex that may be a true catalyst for WOR.[28] The research group also suggested that the heterogeneous catalyst formed *in situ* is unlikely to be ruthenium(IV) oxide hydrate since the highly-hydrated form is susceptible to further oxidation to $RuO_4$, which is inactive toward WOR.[28] Sauvage *et al*. also reported the formation of ruthenium(IV) oxide precipitates from the ruthenium compounds, including $RuCl_3$, $Ru(bpy)_2(CO_3)_2$ in the presence of CAN as the oxidizing agent.[29]

Some transition-metal compounds are irreversibly decomposed to metal oxides under water-oxidation conditions.[30-41] The reported studies of water-oxidizing activities of Mn, Fe, Co, Cu, and Ir compounds under different conditions confirmed that these metal complexes were precatalysts toward WOR.[30-41] However, such results for ruthenium complexes containing oxidizable ligands have not been reported with detail where CAN is used as the sacrificial electron acceptor. Stracke and Finke claimed that the difficulty of identifying $RuO_2$ in the decomposition product triggers some ambiguities in the determination of the true catalyst.[35] On the other hand, the ruthenium complexes are, by far and properly designed, the most stable species reported for WOR.[10-27]

The catalytic activities of RuR and their attributed details have been significantly considered from 1987 by many research groups, which is not the focus of this study.[21,28] Herein, we focused on the obtained solid from the reaction of RuR and CAN. We propose that under water-oxidation conditions, a nano-sized ruthenium-cerium compound is one of the contributors to $O_2$ evolution when RuR and CAN are used as the catalyst and sacrificial electron acceptor, respectively.

## EXPERIMENTAL

### Materials

$[(NH_3)_5RuORu(NH_3)_4ORu(NH_3)_5]Cl_6$ (RuR) and $(NH_4)_2[Ce(NO_3)_6]$ were purchased from Sigma-Aldrich Company. $(NH_4)_2[Ce(NO_3)_5(H_2O)_2]$ was purchased from Santa Cruz Company.

**Procedures**

*Procedure 1*

To explore the characters of the formed solid in the reaction of RuR and CAN, RuR (50.0 mg; 65.1 µmol) was mixed with a 35-fold excess of CAN solution (5.00 mL, 0.40 M). The solid was centrifuged (3000 rpm) for 5 minutes and washed several times with distilled water to remove all the unreacted compounds. No RuR was soluble under these conditions.

*Procedure 2*

RuR (100.0 mg; 130.2 µmol) was mixed with $(NH_4)_2[Ce(NO_3)_5(H_2O)_2]$ as a product of the reduction of CAN (1.0 gr, 1.91 mmol), in 2.00 ml water and stirred for 15 min. For further analysis, the formed solid from the reaction of RuR with $(NH_4)_2Ce(NO_3)_6$ or $(NH_4)_2[Ce(NO_3)_5(H_2O)_2]$ was centrifuged (3000 rpm) for 5 minutes and washed several times with distilled water to remove all the unreacted compounds.

*Procedure 3*

To investigate the nitrate ion from CAN on RuR, RuR (50.0 mg; 65.1 µmol) was dissolved in 10 mL of distilled water. 5 mL of a saturated $NH_4NO_3$ solution, where pH was adjusted to one with nitric acid, was subsequently added to RuR solution. The solid that was obtained from the reaction of RuR, and ammonium nitrate was centrifuged and washed with distilled water.

**Characterization Methods**

The isolated compound in the reaction of RuR with CAN was characterized using a combination of dynamic light scattering (DLS), CHN elemental microanalysis, X-ray diffraction (XRD), high-resolution transmission electron microscopy (HRTEM), X-ray photoelectron spectroscopy (XPS), Fourier transform

infrared spectroscopy (FTIR), UV-Vis spectroscopy, energy dispersive X-ray spectroscopy (EDXS), scanning electron microscopy (SEM), and X-ray absorption near edge structure (XANES). The DLS analysis was conducted using Nicomp 370 DLS particle sizing system. The X-ray diffraction analysis was performed using a Rigaku Ultima IV system. HRTEM was done using an FEI Talos F200X. The XPS analysis was conducted using a PHI 595 multiprobe system. FTIR analysis was performed using a Nicolet 8700 spectrometer. SEM analysis was performed using a JEOL JSM-6335F. The UV-Vis analysis was performed using a Shimadzu UV 2450 spectrometer. X-ray absorption spectra were collected in the transmission mode at the X18A beamline of the National Synchrotron Light Source (NSLS), Brookhaven National Laboratory (BNL). Electrochemical experiments were performed using an EmStat$^{3+}$ from PalmSens Company (the Netherlands).

**Chemical water oxidation**

To elucidate the catalytic behavior of the formed solid in the reaction of RuR and CAN toward WOR, a suspension of the formed product in water was tested by an HQ40d portable dissolved oxygen-meter connected to an oxygen monitor with digital readout at 25 $^{o}$C (Scheme S1). The CAN solution was de-aerated to remove the dissolved oxygen entirely, and 2 mg of the precipitated solid from the reaction of RuR and CAN was added, subsequently. The WOR was confirmed by the onset of oxygen evolution upon the addition of the formed solid to the CAN solution (**Figure 1**). The turnover frequency (TOF) and turnover number (TON) for both RuR and the precipitated solid from the reaction of RuR and CAN are ≈ 0.01 ($mol_{O2}/mol_{RuR}$·s) and ≈ 5 ($mol_{O2}/mol_{RuR}$, for 1000 seconds) in the presence of CAN (0.10 M). Although the TOF and TOF are too small compared to new ruthenium complexes,[18,19] the characterization of the formed solid during the WOR is promising and has rich chemistry of ruthenium complexes during the WOR.

**Results and discussion**

The RuR transformation started occurring immediately after its addition to CAN solution. The nanoparticles inception and agglomeration were monitored by dynamic light scattering (DLS) during the reaction (Figure S1(a-c)). After one minute of the reaction, DLS analysis showed the formation of particles in the range of 100 nm. However, after a few minutes, more agglomeration occurred, and larger particles were observed. This analysis revealed the formation and significant growth of the particles over time.

CHN microanalysis was used to conduct a comparison between RuR and the product of its reaction with CAN regarding their nitrogen contents. **Table 1** shows the results of the nitrogen contents of RuR, and the precipitated solid. CHN analysis confirmed that the precipitate obtained from the reaction of RuR and CAN could not be $RuO_2$, since the elemental composition of this compound did not show any nitrogen loss. Even, CHN microanalysis results showed that the nitrogen content of the newly formed compound (24.6% nitrogen) was a little higher than that of RuR (22.9% nitrogen), which implied that no significant $RuO_2$ presents on the catalyst and that another nitrogen source has been added to the compound. The higher nitrogen content in the precipitate than in RuR may be attributed to the presence of nitrate ions liberated from the CAN hydrolysis.

The product of the reaction of RuR and CAN was isolated at different times of the reaction and further analyzed by XRD. The dominant peaks in the XRD of the as-formed solid, as well as the solid even after 5 hours of the reaction, match fairly well with the diffraction patterns of pristine RuR (**Figure 2(a-c)**). Since the RuR can be oxidized reversibly to ruthenium brown ($[(NH_3)_5RuORu(NH_3)_4ORu(NH_3)_5]^{7+}$),[28] the changes in XRD patterns of RuR after the CAN addition may account for this conversion. However, the main features of the diffraction patterns were preserved while their intensities changed due to changes in the size distribution of the nanoparticles. In the early steps of the reaction, the XRD patterns showed peaks with the low intensities and relatively large FWHM values (**Figure 2 (b)**). The XRD patterns for the sample obtained after 5 hours of reaction showed narrower, more intense peaks (**Figure 2(c)**). The individual effect of nitrate ions on the electrostatic agglomeration of the RuR was also tested using

ammonium nitrate as the source. The XRD patterns of the solid isolated from the reaction of RuR and $NH_4NO_3$ are shown in **Figure 2(d)** (procedure 3), and these confirm that the RuR/brown crystalline structure is retained.

For further analysis, RuR and the solid formed from its reaction with CAN and $NH_4NO_3$ were analyzed separately by HRTEM. HRTEM of the pure RuR revealed the presence of < 3nm crystalline colloidal nanoparticles dispersed in an amorphous RuR matrix. The d-spacing measurements from the lattice fringes in the crystalline nanoparticles give values of 0.28 nm ($2\Theta = 32^o$), which is consistent with the crystal structure of RuR (**Figure 3(a-c)**).

HRTEM images of the solid obtained from the reaction of the RuR with CAN show clear lattice fringes with inter-planar distances of 0.28 ($2\Theta = 32^o$), 0.34 ($2\Theta = 26^o$), and 0.17 nm ($2\Theta = 52^o$) (**Figure 4(a-c)**). The d-spacings of 0.17 and 0.34 nm are consistent with values reported for inter-planar spacings in Ce(III) oxide and an oxygen-deficient ceria ($CeO_{1.695}$).

As discussed earlier, the precipitate that had been formed from the reaction of RuR and ammonium nitrate (procedure 3) was also analyzed by HRTEM to explore the effect of nitrate ions on the aggregation of the preexisting nanoparticles. HRTEM images of the reaction product of RuR with ammonium nitrate show crystalline nanoparticles ~3 nm in diameter, embedded in an amorphous matrix (**Figure 5(a-d)**). Fast Fourier transform (FFT) analysis of the crystalline areas confirms that, here again, the d-spacing of the particles is 0.28 nm. This result is also consistent with the XRD patterns from the product obtained from the reaction of RuR and $NH_4NO_3$.

Surface plots of the precipitated solids showed that number densities of the crystalline nanoparticles in the reaction products of RuR with CAN and ammonium nitrate were much higher than that for bare RuR, most probably due to the electrostatic forces between ions ((Figure S2 (I-III)).

To further reveal the surface chemistry of RuR and the product of its reaction with CAN, XPS analysis was done (**Figure 6,7**). Since samples were exposed to air, the binding energies were calibrated against the binding energy of adventitious carbon (284.8 eV). The survey spectrum from the RuR revealed the

presence of ruthenium, chlorine, nitrogen, and oxygen. However, the survey spectrum from the compound produced by the reaction of RuR and CAN also showed the existence of a small amount of cerium (0.85 atomic percent). To shed light on the oxidation states of different elements in RuR before and after the reaction with CAN, high-resolution spectra of ruthenium, nitrogen, oxygen, and cerium were deconvoluted using the synthetic peaks. Since the deconvolution of the Ru 3d is not easy due to the overlap of C 1s and Ru 3d core levels, oxidation states of ruthenium have been obtained from studying the Ru 3p core level. The deconvoluted Ru $3p_{3/2}$ peak of RuR represents two regions corresponding to Ru(III) $3p_{3/2}$ and Ru(IV) $3p_{3/2}$ at 462.5 and 464.5 eV, respectively. The ratio of the Ru(III) $3p_{3/2}$ to Ru(IV) $3p_{3/2}$ regions for RuR was 1.35. The Ru $3p_{3/2}$ peak for the product of the reaction of RuR with CAN was also deconvoluted using two synthetic peaks belonging to Ru(III) $3p_{3/2}$ (463.6 eV) and Ru (IV) $3p_{3/2}$ (465.5 eV). Although a shift in the Ru 3p peak toward higher binding energy was observed after the reaction, the ratio of Ru(III) $3p_{3/2}$ to Ru(IV) $3p_{3/2}$ was not changed significantly (1.27). The slight change in the oxidation states ratio and the binding energy shift corresponds to partial oxidation of Ru(III) to Ru(IV). The high-resolution spectra of N 1s were also analyzed for RuR before and after the reaction with CAN to investigate the nature of nitrogen contents in these samples. The N 1s spectrum of RuR was deconvoluted using a single peak with FWHM of 2.5 and binding energy of ~ 399 eV. This peak corresponds to the ammonia ligands in RuR. The N 1s of RuR after the reaction with CAN was substantially broadened due to the presence of more than one type of nitrogen.

Two peaks with binding energies of ~ 399 and 400 eV were assigned to ammonia ligands and free entangled ammonium ions, respectively. Another peak was also observed at ~ 407 eV, which confirmed the presence of nitrate ions. The O 1s spectra from these two compounds were also compared to further investigate the different oxygen species. The O 1s spectrum of the RuR was deconvoluted into three regions related to O-Ru (529.3 eV), O-C (531.0 eV), and O=C (532.2 eV). For the product obtained from the reaction of RuR and CAN, the O 1s spectrum presented a relatively broad peak. This slight broadening was due to the formation of cerium oxides. Therefore, the high-resolution O 1s spectrum of

this compound showed four peaks at ~ 529.0, 530.0, 531.4, and 533.1 eV corresponding to O-Ce, O-Ru, O-C, and O=C, respectively. The survey spectrum of the precipitated solid also revealed the existence of a small amount of cerium (0.85%). For further clarification, a high-resolution spectrum of cerium was obtained using the pass energy of 50 eV. According to the results from XRD and HRTEM, Ce 3d peaks were deconvoluted into two peaks belonging to a Ce(III) compound and Ce(IV). The results obtained from the XPS analysis confirmed that a ruthenium compound could precipitate in the presence of $[Ce(NO_3)_5(H_2O)_2]^{2-}$ and nitrate ions.

FTIR study was done to provide complementary data regarding the analogy between the molecular structure of RuR and the solid obtained from the reaction of RuR and CAN (**Figure 8** (**a,b**)). The FTIR spectrum of the solid precipitated in the reaction of RuR with CAN showed similar absorption bands to that obtained from RuR. However, the peaks at 1382, 1050, 820 $cm^{-1}$ showed the presence of nitrate ions in the precipitate.[42] These three peaks stand for antisymmetric stretching, symmetric stretching, and out-of-plane bending of nitrate ions, respectively.[42] The first peak appearing at 3453 $cm^{-1}$ belongs to the O-H stretching of either adsorbed or hydrated water absorption bands.[42] The N-H stretching vibrations appeared at 3268 and 3131 $cm^{-1}$ for RuR. The obtained solid from the reaction of RuR and $(NH_4)_2[Ce(NO_3)_5(H_2O)_2]$ (procedure 2), showed similar peaks with the product of the reaction of RuR and CAN (**Figure 8(c)**). The peak at 1625 $cm^{-1}$ belongs to the degenerate deformation vibration whereas the peak at 1292 $cm^{-1}$ is attributed to the symmetric deformation of $NH_3$ attached to Ru(III). The peak at 804 $cm^{-1}$ (**Figure 8(a)**) corresponds to the $NH_3$ rocking bands in the RuR complex, which is absent in the FTIR spectra from the two other solids (**Figure 8 (b,c)**) obtained from the reactions of RuR with CAN and $(NH_4)_2[Ce(NO_3)_5(H_2O)_2]$. The absence of this peak suggests the formation of the oxidized form of RuR (ruthenium brown). The ruthenium-nitrogen stretching vibration is expected to occur at frequencies below 600 $cm^{-1}$.

The STEM-EDXS analysis was performed to study the chemical composition and elemental distribution of the ruthenium compounds. **Figures 9** and **10** are examples of elemental mapping data from RuR and

the product of its reaction with CAN, respectively. The results of EDXS microanalysis did not show a significant change in the chemical composition before and after the precipitation except for cerium and oxygen (Table S1). The emergence of cerium and the elevated oxygen content were due to the addition of CAN and the subsequent formation of cerium oxides. The presence of chloride in the precipitate formed in the reaction of RuR and CAN is another evidence for the conservation of the RuR structure. EDXS is not a good method to measure N content, but in contrast to CHN microanalysis, and based on EDXS results the nitrogen content in the precipitated solid (procedure 1) sample is lower than in RuR (Table S1). It seems that the cerium compounds cover the RuR structure in the precipitated solid (procedure 1).

**Figure 11 (a**,**b**) are representative secondary electron SEM images showing the morphologies of RuR and the product isolated from its reaction with CAN. At high magnification, the RuR showed a layered structure. However, this layered structure is better defined for the solid resulting from the reaction of RuR and CAN, where the stacking of layers is observed.

The UV-Vis spectra of the solid obtained by the reaction of RuR and CAN in water at 40 $^{o}$C shows two dominant absorption bands at 355 and 536 nm (**Figure 12a**). Both bands are related to two intense absorptions of the RuR.[28] An increase in temperature is necessary to solubilize the solid and obtain the spectrum. On the other hand, cyclic voltammograms of the precipitated solid from the reaction of RuR and CAN, and RuR in $HNO_3$ (0.10 M) at 40 $^{o}$C show similar peaks corresponding to Ru(II)/Ru(III) for both compounds. The precipitated solid from the reaction of RuR and CAN in addition to the related peaks for Ru(II)/Ru(III) also show also a reduction peak related to Ce(IV)/(III) reduction (**Figure 12b**). The precipitated solid from the reaction of RuR and CAN at least contains both cerium and RuR.

X-ray absorption spectroscopy as an element-specific technique was performed to determine the oxidation state of the isolated product from the reaction of RuR with CAN. A Silicon (111) channel-cut double crystal monochromator was used to monochromatize the synchrotron radiation. The incident and transmitted beam intensities were monitored using ionization chambers filled with a mixture of Ar

and He gases. The samples were diluted by h-BN and ground well by mortar and pestle, and then pressed into pellets. Then the beamline energy was shifted to measure the K-edge of Ru. Athena software was used for data analysis where the background, post, and pre-edge corrections were made. To analyze the edge energy and white line intensity of the newly formed solid, ruthenium foil and ruthenium(IV) oxide standard samples were used as references. **Figure 13** shows the XANES regions for the precipitated solid and two reference samples. Ruthenium K-edge for ruthenium foil showed an absorption maximum located at 22117 eV, which agrees with literature data.[43] The edge energy for ruthenium(IV) oxide and the formed solid were located around 22125 eV. Although these two samples showed very close edge energies, they are significantly different regarding the white-line intensities. The much lower white-line intensity from the obtained solid indicated that this sample is less oxidized than a standard ruthenium(IV) oxide. The XANES results supported this hypothesis that the ruthenium species in the obtained solid from the reaction of RuR and CAN was not only a ruthenium(IV) species. The XANES results suggest a mixture of Ru(III) and Ru(IV) in the formed precipitate. Other than the difference in white-line intensity, the obtained solid showed pre-edge features that were absent in ruthenium(IV) oxide and ruthenium foil. In crystalline ruthenium(IV) oxide, the ruthenium(IV) ion is bonded to six oxygen atoms in an octahedral arrangement. Therefore, no pre-edge feature which normally originates from the distortion in complex geometry and hybridization of orbitals allowing dipole forbidden transitions (1s -> 4d) can be observed in symmetric complexes such as ruthenium(IV) oxide.[44] In contrast to ruthenium(IV) oxide, the presence of the pre-edge features in our proposed catalyst indicates a change in the type and geometry of ligands around the ruthenium center.

The results obtained from detailed analyses of the precipitate formed in the reaction of RuR with CAN applied in WORs suggest the emergence of stabilized ruthenium–cerium nanoparticles. A homogeneous RuR catalyst is partially oxidized in the presence of CAN and a mixture of RuR/brown forms subsequently. The RuR/brown mixture with a high positive charge is expected to be very reactive to the negative charge on $[Ce(NO_3)_5(H_2O)_2]^{2-}$,[45] which forms due to the reduction of CAN. In the presence of

$[Ce(NO_3)_5(H_2O)_2]^{2-}$ (Figure S4) or nitrate ions, a RuR/brown mixture can be precipitated electrostatically, forming nanoparticles. XRD analysis also confirmed this hypothesis by showing diffraction patterns corresponding to $[Ce(NO_3)_5(H_2O)_2]^{2-}$ (JCPDS Card No. 98-009-6585) (Figure S3). HRTEM, which is a robust and widely used method to distinguish the presence of nanoclusters, helped us to detect the pre-existing nanoclusters in the RuR. Based on the HRTEM results for RuR, the positively charged ruthenium nanoclusters ($[(NH_3)_5RuORu(NH_3)_4ORu(NH_3)_5]^{6+}$) have been stabilized in an amorphous matrix due to the presence of chloride as an anion. However, following the addition of CAN to the RuR solution, three effects may be triggered: i) partial oxidation of RuR to ruthenium brown; ii) reduction of CAN to $(NH_4)_2[Ce(NO_3)_5(H_2O)_2]$ and liberation of nitrate ions; iii) agglomeration of colloidal RuR/brown nanoclusters in the presence of nitrate and $[Ce(NO_3)_5(H_2O)_2]^{2+}$ ions. The retention of the 0.28 nm d-spacing in most regions of the solid implies that the pre-existing primary nanoparticles in RuR had been electrostatically aggregated during the reaction of RuR with CAN. As the surface plots also showed, there are higher populations of nanoparticles in the presence of CAN compared to RuR in regions with equal areas; this is presumably due to the electrostatic attractions between the positively-charged RuR/brown nanoclusters and negative charges on cerium and nitrate species. Such studies are important in order to recognize the true catalyst. As an example, Brudvig's and Crabtree's groups reported that an efficient catalyst for the WOR is formed by simple anodic deposition from Cp*Ir aqua or hydroxo complexes; the catalyst is robust and stable for the water-oxidation reaction and consists of iridium and oxygen.[46,47]

**Conclusions**

In this work, it is suggested that the products of the hydrolysis of CAN in a reaction with RuR result in the formation and agglomeration of Ru-Ce based nanoparticles, which are one of the candidates for the true catalyst for WOR. The positively charged RuR/brown nanoclusters are precipitated in the presence of anionic species, including $NO_3^-$, $[Ce(NO_3)_6]^{2-}$, and the hydrolyzed form of the CAN ($[(Ce(NO_3)_5(H_2O)]^{2-}$).

Thus, a nanosized Ru-Ce compound precipitated by $[(Ce(NO_3)_5(H_2O)_2]_{2-}$ and $NO_3^-$, is a possible contributor to WOR in the reaction and now is a candidate as a contributor to the observed WOR. Electrostatic stabilization of the charged colloidal ruthenium particles by anionic cerium-based species is a crucial breakthrough in WOR and artificial photosynthesis since the results can be applied in the design and synthesis of new catalysts. However, the question remains open about how critical the role of $[Ce(NO_3)_5(H2O)_2]^{2-}$ is in forming the true catalyst.

AUTHOR INFORMATION

ACKNOWLEDGMENT

MMN, BS and SMH are grateful to the Institute for Advanced Studies in Basic Sciences. SLS thanks the U.S. Department of Energy, Office of Basic Energy Sciences, Division of Chemical, Geochemical and Biological Sciences (under Grant DE-FG02-86ER13622.A000). The electron microscopy studies were performed using the facilities in the UConn/Thermo Fisher Scientific Center for Advanced Microscopy and Materials Analysis (CAMMA).

**References**

1 N. S. Lewis and D. G. Nocera, *Proc. Natl. Acad. Sci. USA,* 2006, **103**, 15729.

2 M. Z. Jacobson, *Energy Environ. Sci.*, 2009, **2**, 148.

3 J. Barber, *Chem. Soc. Rev.*, 2009, **38**, 185.

4 M. D. Kärkäs, O. Verho, E. V. Johnston and B. Åkermark, *Chem. Rev.*, 2014, **114**, 11863.

5 T. Jafari, E. Moharreri, E., A. S. Amin, R. Miao, W. Song, and S. L. Suib, *Molecules,* 2016, **21**, 900.

6 A. Singh and L. Spiccia, *Coord. Chem. Rev*. 2013, **257**, 2607.

7 W. Ruttinger and G. C. Dismukes, *Chem. Rev.* 1997, **97**, 1.

8 M. Yagi and M. Kaneko, *Chem. Rev*. 2001, **101**, 21.

9 M. M. Najafpour, G. Renger, M. Hołyńska, A. N. Moghaddam, E.-M. Aro, R. Carpentier, H. Nishihara, J. J. Eaton-Rye, J.-R. Shen and S. I. Allakhverdiev, *Chem. Rev.*, 2016, **116**, 2886.

10 M. Hirahara, A. Shoji and M. Yagi, *Eur. J. Inorg. Chem*., 2014, **4**, 595.

11 S. Neudeck, S. Maji, I. Lopez, S. Meyer, F. Meyer and A. Llobet, *J. Am. Chem. Soc.*, 2014, **136**, 24.

12 I. Lopez , M. Z. Ertem, S. Maji , J. Benet-Buchholz, A. Keidel, U. Kuhlmann, P. Hildebrandt, C. J. Cramer, V. S. Batista and A. Llobet, *Angew. Chem. Int. Ed.,* 2014, **53**, 205.

13 L. Duan, L. Wang, A. K. Inge, A. Fischer, X. Zou and L. Sun, *Inorg. Chem.,* 2013, **52**, 7844.

14 Y. Gao, X. Ding, J. Liu, L. Wang, Z. Lu, L. Li and L. Sun, *J. Am. Chem. Soc.,* 2013, **135**, 4219.

15 F. Li, B. Zhang, X. Li, Y. Jiang, L. Chen, Y. Li and L. Sun*, Angew. Chem. Int. Ed.,* 2011, **50**, 12276.

16 J. K. Hurst, *Coord. Chem. Rev.,* 2005, **249**,313.

17 J. A. Stull, R. D. Britt, J. L. McHale, F. J. Knorr, S. V. Lymar and J. K. Hurst, *J. Am. Chem. Soc.,* 2012, **134**, 19973.

18 L. Duan, F. Bozoglian, S. Mandal, B. Stewart, T. Privalov, A. Llobet and L. Sun, *Nat. Chem*. 2012, **4**, 418.

19 C. J. Richmond, R. Matheu, A. Poater, L. Falivene, J. Benet-Buchholz, X. Sala, L. Cavallo and A. Llobet, *Chem. Eur. J.,* 2014, **20**, 1.

20 J. A. Gilbert, D. S. Eggleston, W. R. Murphy Jr., D. A. Geselowitz, S. W. Gersten, D. J. Hodgson and T. J. Meyer, *J. Am. Chem. Soc*., 1985, **107**, 3855.

21 R. Ramaraj, A. Kira and M. Kaneko, *Angew. Chem. lnt. Ed.,* 1986, **25**, 1009.

22 D. A. Geselowitz, W. Kutner and T. J. Meyer, *Inorg. Chem.*, 1986, **25**, 2015.

23 J. E. Earley, P. M. Smith, T. Fealey and J. V. Silverton, *Inorg. Chem.,* 1971, **10**, 1943.

24 J. E. Earley and T. Fealey, *Inorg. Chem*., 1973, **12**, 323.

25 J. A. Baumann and T. J. Meyer, *Inorg. Chem.*, 1980, **19**, 345.

26 H.N. Kagalwala, L.Tong, R. Zong, L. Kohler, M. SG. Ahlquist, T. Fan, K. J. Gagnon and R. P. Thummel, *ACS Catal.*, 2017, **7**, 2607.

27 P. Garrido-Barros, C. Gimbert-Suriñach, R. Matheu, X. Sala and A. Llobet, *Chem. Soc. Rev.,* 2017, **46**, 6088.

28 A. Mills and T. Russell, *J. Chem. Soc. Faraday Trans*. 1991, **87**, 313.

29 J. P. Collin and J. P. Sauvage, *Inorg. Chem.,* 1986, **25**, 135.

30 M. M. Najafpour and H. Feizi, *Catal. Sci. Technol*., 2018, **8**, 1840.

31 M. M. Najafpour and H. Feizi, *Dalton Trans.*, 2018, **47**, 6519.

32 M. M. Najafpour, F. Ebrahimi, R. Safdari, M. Z. Ghobadi, M. Tavahodi and P. Rafighi, *Dalton Trans*., 2015, **44**, 15435.

33 M. M. Najafpour and A. N. Moghaddam, *Dalton Trans.*, 2012, **41**, 10292; M. M. Najafpour, M. Hołyńska, A. N. Shamkhali, S. H. Kazemi, W. Hillier, E. Amini, M. Ghaemmaghami, D. J. Sedigh, A. N. Moghaddam, R. Mohamadi, S. Zaynalpoor and K. Beckmann, *Dalton Trans*., 2014, **43**, 13122.

34 M. M. Najafpour, R. Safdari, F. Ebrahimi, P. Rafighi and R. Bagheri, *Dalton Trans.*, 2016, **45**, 2618.

35 J. J. Stracke and R. G. Finke, *ACS Catal.*, 2014, **4**, 909.

36 V. Artero and M. Fontecave, *Chem. Soc. Rev*., 2013, **42**, 2338.

37 D. Hong, J. Jung, J. Park, Y. Yamada, T. Suenobu, Y.-M. Lee, W. Nam and S. Fukuzumi, *Energy Environ. Sci*., 2012, **5**, 7606.

38 N. D. Schley, J. D. Blakemore, N. K. Subbaiyan, C. D. Incarvito, F. D'Souza, R. H. Crabtree and G. W. Brudvig, *J. Am. Chem. Soc.*, 2011, **133**, 10473.

39 X. Liu, H. Jia, Z. Sun, H. Chen, P. Xu and P. Du, *Electrochem. Commun*., 2014, **46**, 1.

40 M. M. Najafpour, A. N. Moghaddam, H. Dau and I. Zaharieva, *J. Am. Chem. Soc.* 2014, **136**, 7245.

41 S. Fukuzumi and D. Hong, *Eur. J. Inorg. Chem*., 2014, **4**, 645.

42 K. Nakamoto, Infrared and Raman spectra of inorganic and coordination compounds, sixth edition, *A Wiley-Interscience Publication*, 2009.

43 A. Kar, A. Kundu, S. Bhattacharyya, S. Mandal and A. Patra. *RSC Adv.*, 2013, **3**, 13372.

44 J. A. Bearden and A. F. Burr, *Rev. Mod. Phys.*, 1967, **125**, 19.

*45* M. Najafpour and P. Starynowicz*, Acta Cryst.*, 2006, **E62**, i145.

46 J. D. Blakemore, N. D. Schley, G. W. Olack, C. D. Incarvito, G. W. Brudvig and R. H. Crabtree, *Chem. Sci*., 2011, **2**, 94.

47 J. D. Blakemore, N. D. Schley, M. N. Kushner-Lenhoff, A. M. Winter, F. D'Souza, R. H. Crabtree and G. W. Brudvig, *Inorg. Chem*., 2012, **51**, 7749.

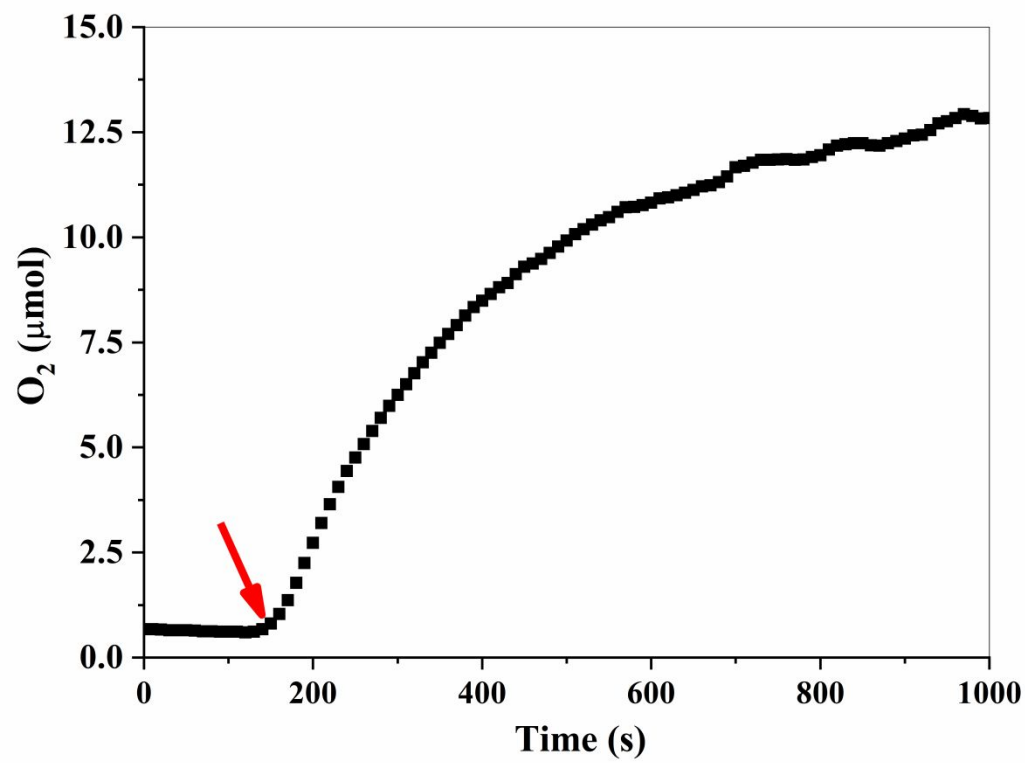


**Figure 1.** Oxygen-evolution reaction conducted by the isolated solid by the procedure 1 and CAN (40 ml, 0.11M) at 25°C. The red arrow indicates the time of adding of the catalyst (2.0 mg) to CAN.

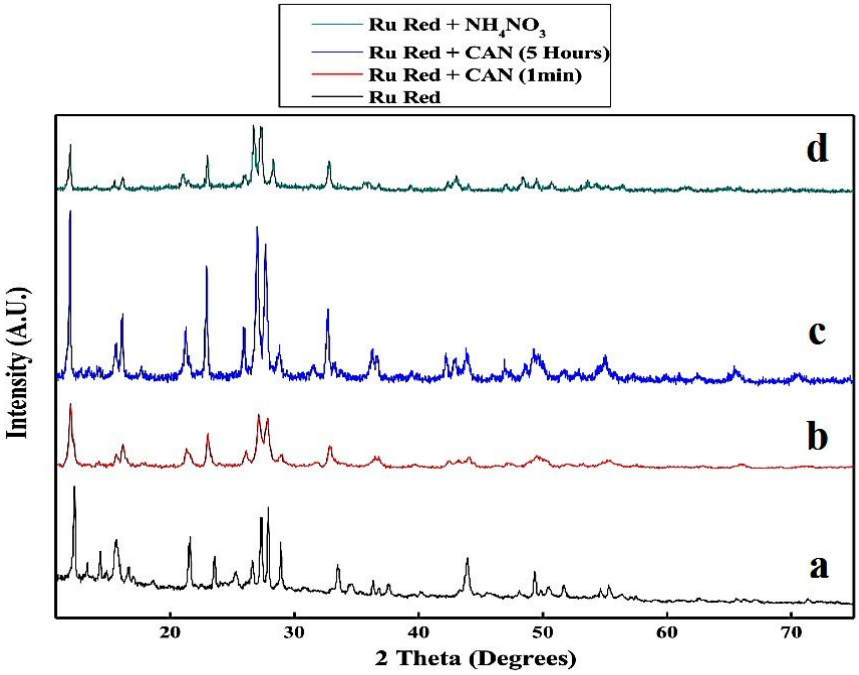


**Figure 2.** XRD patterns of (a) RuR (b) As formed solid from the reaction of RuR and CAN (c) the isolated precipitate after 5 hours of the reaction between RuR and CAN (d) the obtained solid from the reaction of RuR and $NH_4NO_3$.

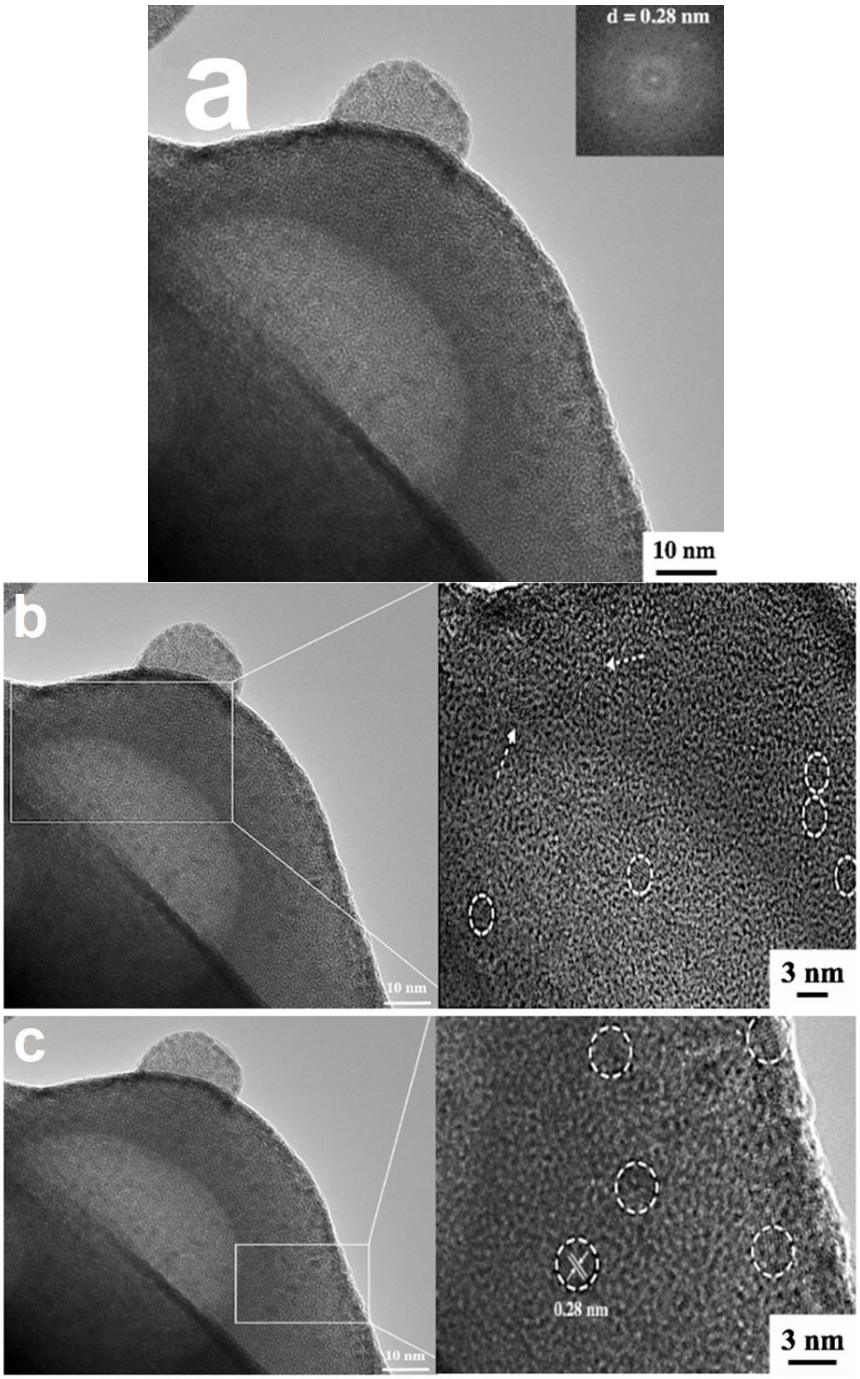
a
d = 0.28 nm
10 nm
b
10 nm
3 nm
c
10 nm
0.28 nm
3 nm

**Figure 3.** HRTEM images (a) and FFT pattern of RuR (b,c). Magnified HRTEM images at different regions show nanoparticles of < 3nm.

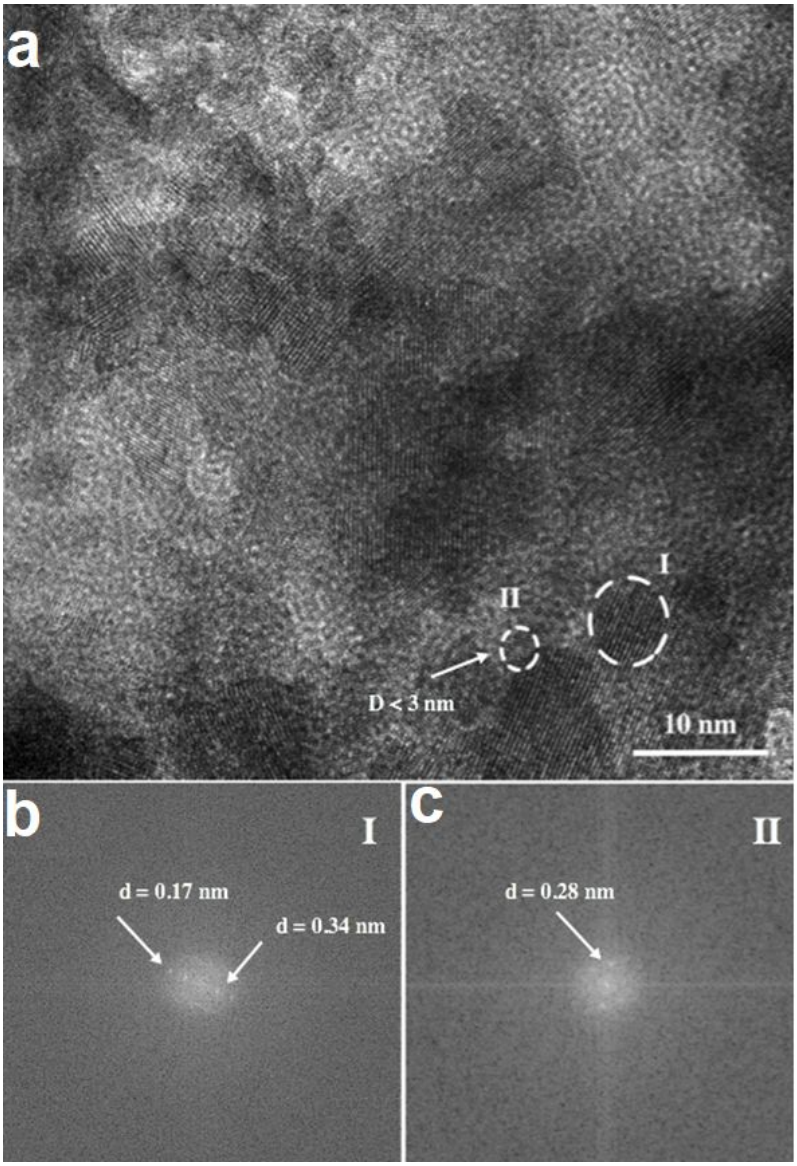

**Figure 4.** HRTEM images of the obtained product from the reaction of RuR and CAN (a). FFT pattern of region I shows d-spacing of 0.17 and 0.34 nm (b). FFT pattern of region II shows d-spacing of 0.28 nm (c).

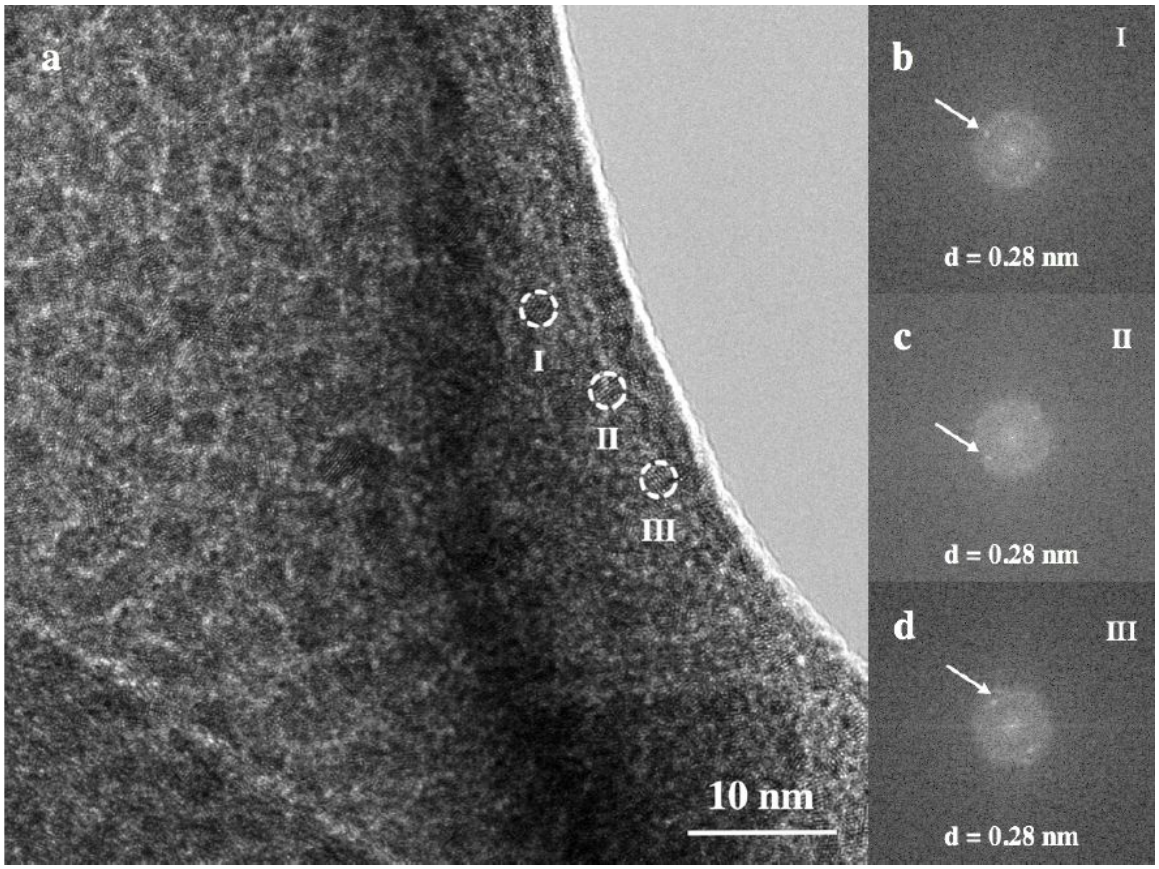


**Figure 5** HRTEM of the precipitate obtained from the reaction of RuR and $NH_4NO_3$ (a). FFT pattern of regions I-III (b-d).

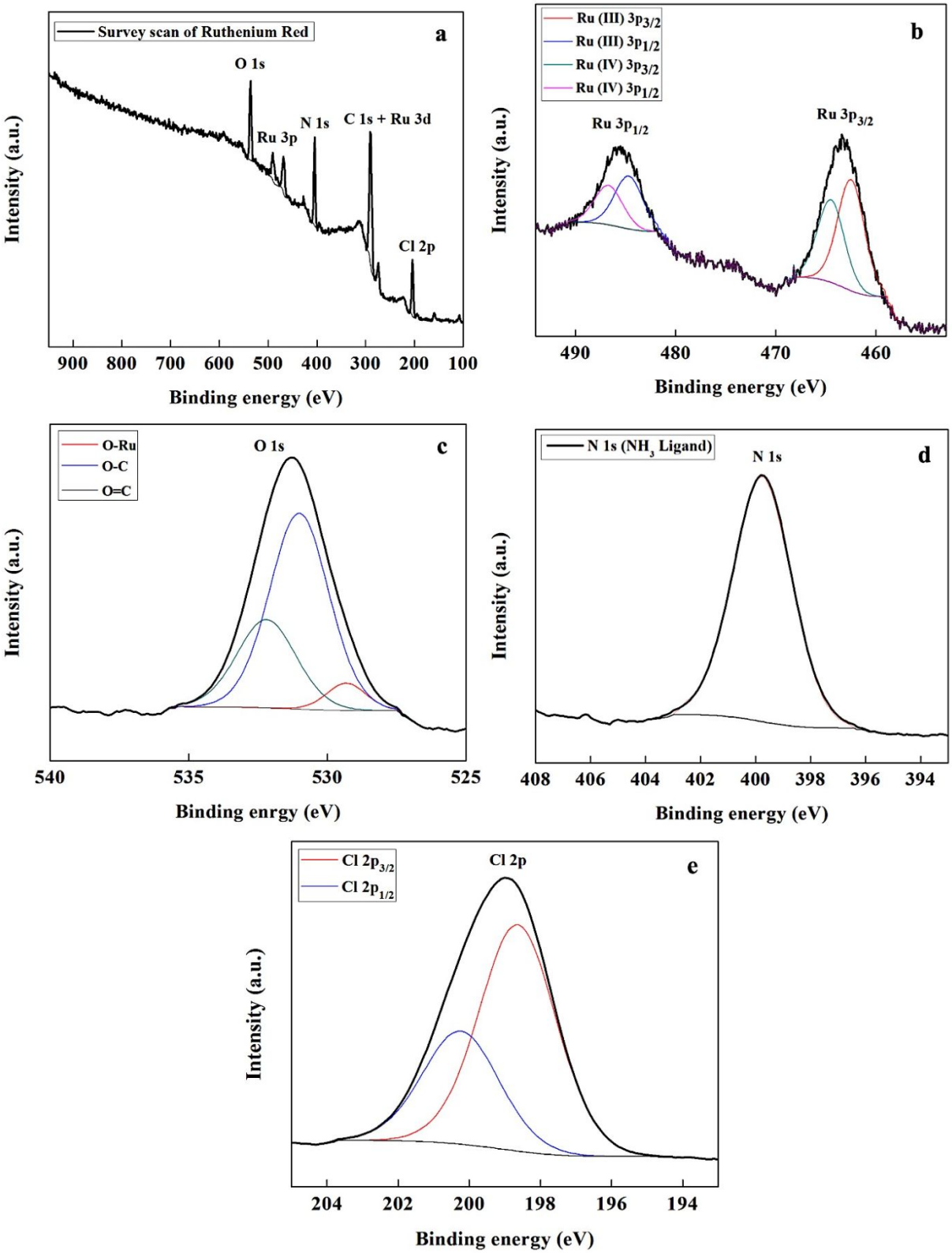
Survey scan of Ruthenium Red
a
O 1s
Ru 3p
N 1s
C 1s + Ru 3d
Cl 2p
Intensity (a.u.)
900 800 700 600 500 400 300 200 100
Binding energy (eV)
Ru (III) 3p3/2
Ru (III) 3p1/2
Ru (IV) 3p3/2
Ru (IV) 3p1/2
b
Ru 3p1/2
Ru 3p3/2
Intensity (a.u.)
490 480 470 460
Binding energy (eV)
O-Ru
O-C
O=C
O 1s
c
Intensity (a.u.)
540 535 530 525
Binding enrgy (eV)
N 1s (NH3 Ligand)
N 1s
d
Intensity (a.u.)
408 406 404 402 400 398 396 394
Binding energy (eV)
Cl 2p3/2
Cl 2p1/2
Cl 2p
e
Intensity (a.u.)
204 202 200 198 196 194
Binding energy (eV)

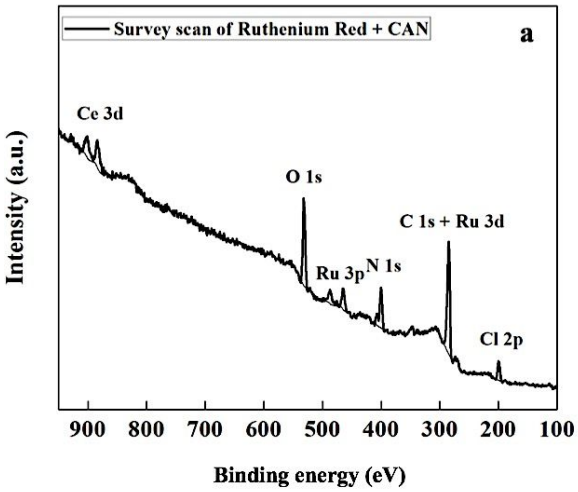


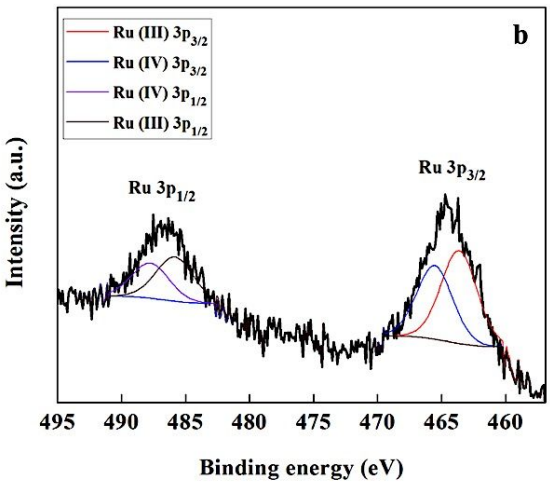


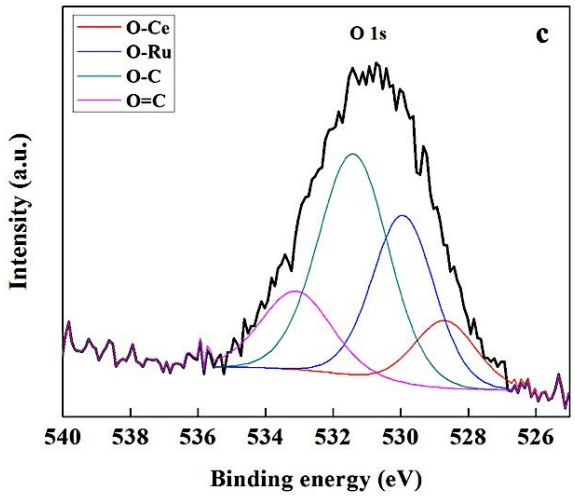


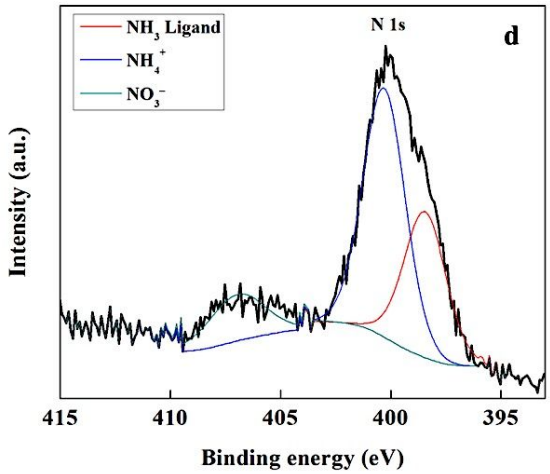


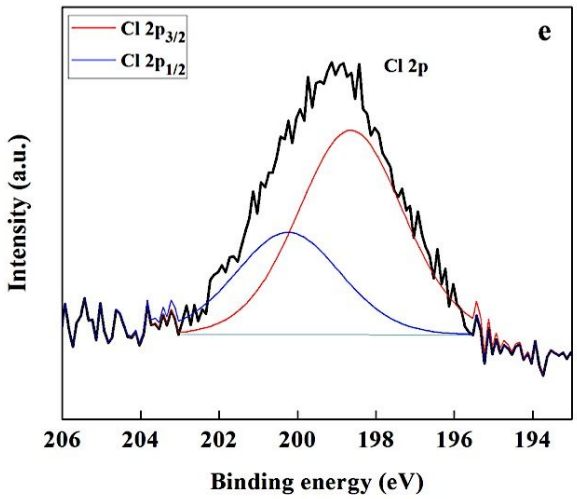


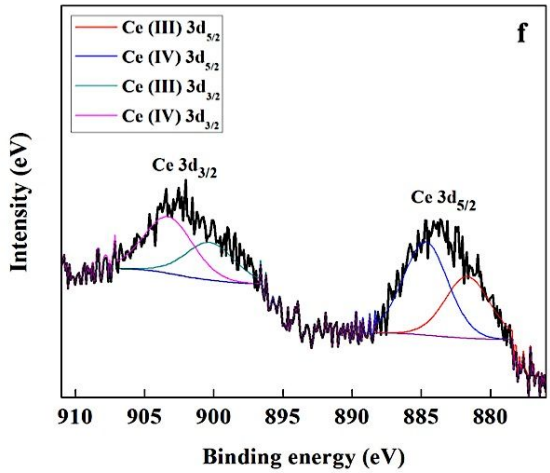


**Figure 6.** XPS spectra of (a) the survey scan (b) Ru 3p (c) O1s (d) N 1s (e) Cl 2p of RuR.

**Figure 7.** XPS spectra of (a) the survey scan (b) Ru 3p (c) O1s (d) N 1s (e) Cl 2p (f) Ce 3d of the solid obtained from the reaction of RuR and CAN.

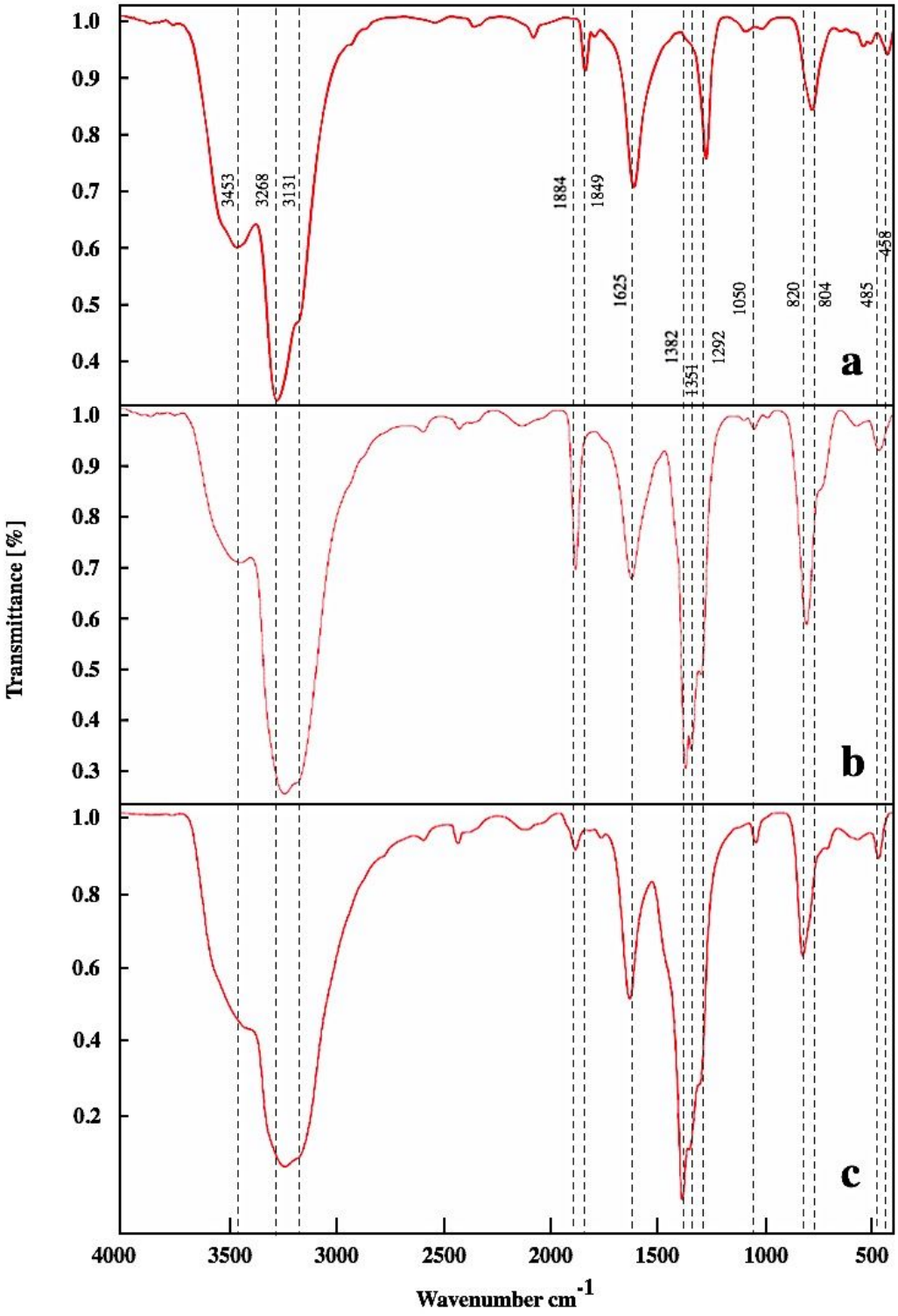


**Figure 8.** FTIR spectra of RuR (a), the precipitated solid from the reaction of RuR with CAN (b), isolated solid from the reaction of RuR and $(NH_4)_2[Ce(NO_3)_5(H_2O)_2]$ (c).

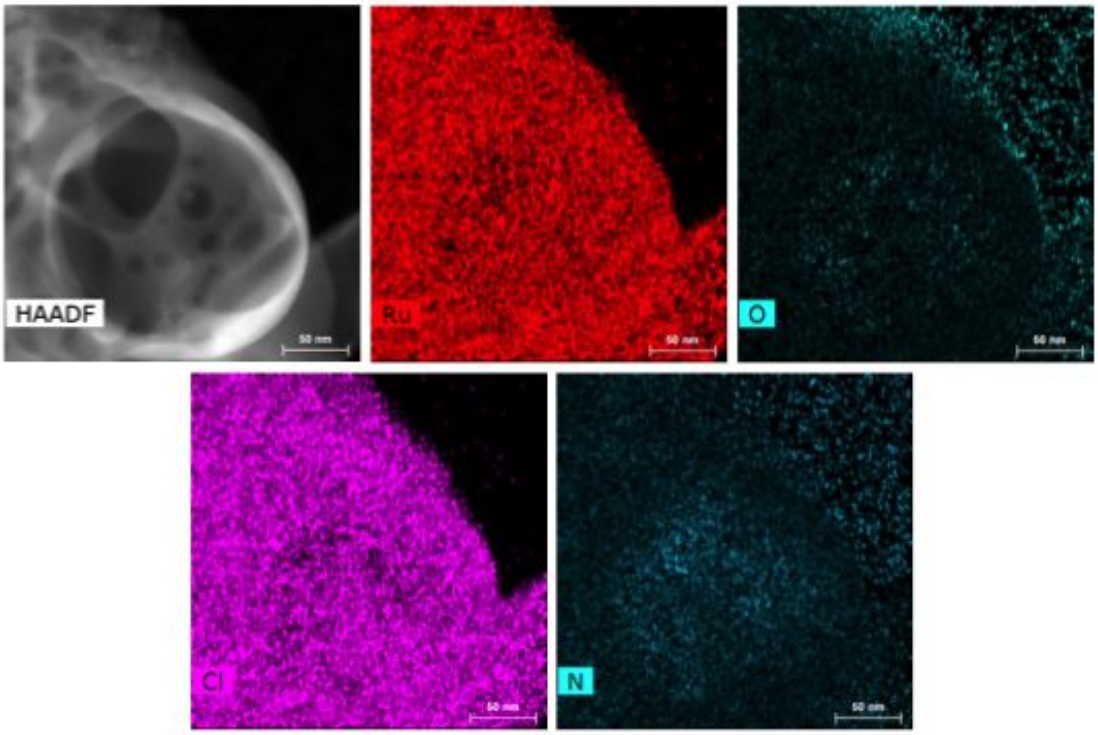


**Figure 9.** The energy dispersive X-ray (EDX) mapping analysis of RuR.

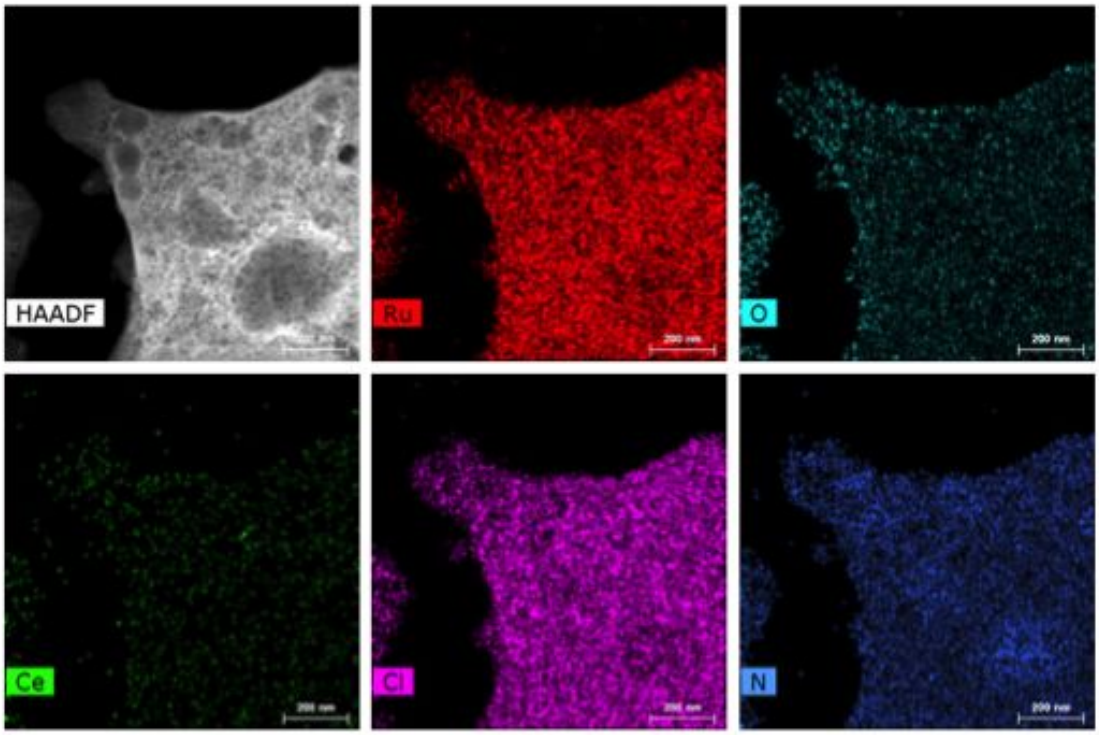


**Figure 10.** The energy dispersive X-ray (EDX) mapping analysis of isolated solid from the reaction of RuR and CAN.

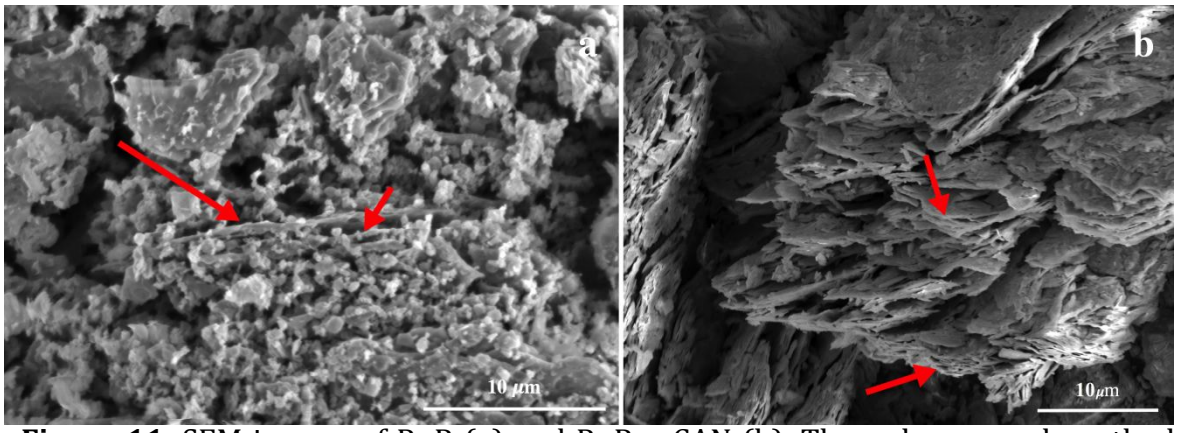


**Figure 11.** SEM images of RuR (a) and RuR + CAN (b). The red arrows show the layered microstructures.

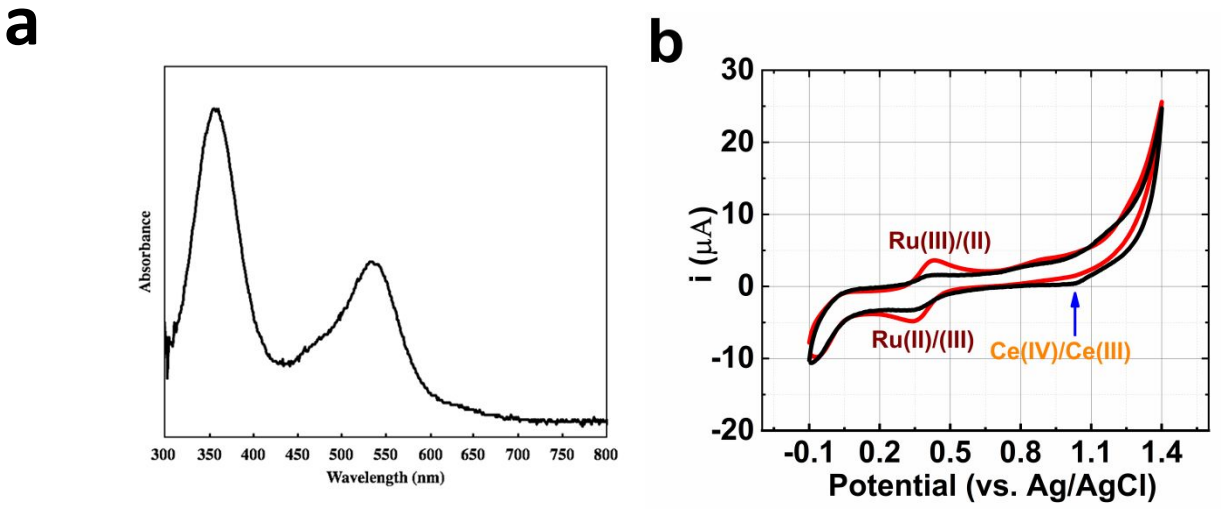


**Figure 12.** UV-Vis spectrum of the precipitated solid from the reaction of RuR and CAN in water at 40 $^{0}$C. The solid at 40 $^{0}$C is relatively soluble in water to obtain UV-Vis spectrum (**a**). Cyclic voltammograms of the precipitated solid from the reaction of RuR and CAN (black) and RuR (red) in water at 40 $^{0}$C (b). The solid at 40 $^{0}$C is relatively soluble in water to obtain cyclic voltammogram. Cyclic voltammogram is recorded in $HNO_3$ (0.10 M) using fluorine-doped tin oxide (FTO), Pt foil and, Ag/AgCl as working, counter, and reference electrodes, respectively.

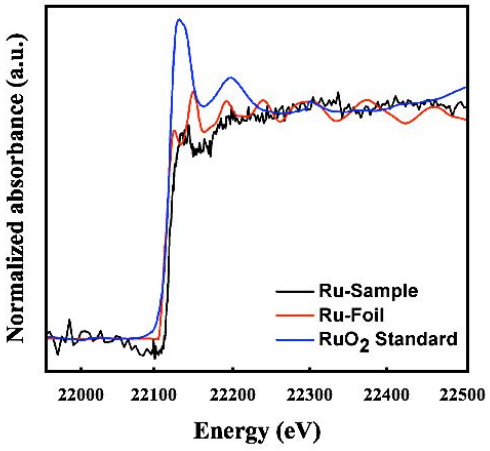


**Figure 13.** Ru K-edge XANES spectrum of the product of the reaction of RuR with CAN in comparison with the standard $RuO_2$ and ruthenium foil samples.

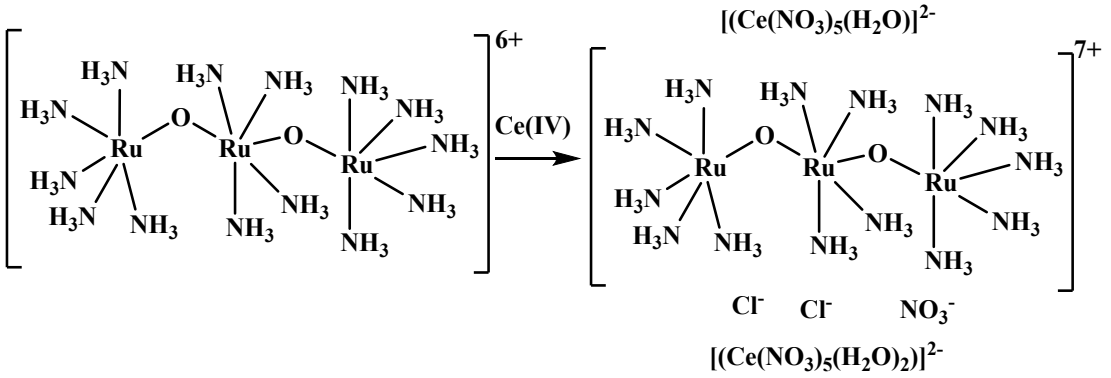


**Scheme 1.** Proposed reaction mechanism in the reaction of RuR with an excess amount of CAN.

| Sample ID | H(wt%) | | N(wt%) | |
|---|---|---|---|---|
| | Calc. | Found | Calc. | Found |
| RuR | 5.87 | 5.70 | 22.9 | 22.9 |

| | | | | |
|---|---|---|---|---|
| Precipitated Solid | - | 4.71 | - | 24.6 |

**Table 1.** CHN microanalysis for RuR and the precipitated solid obtained from its reaction with CAN.

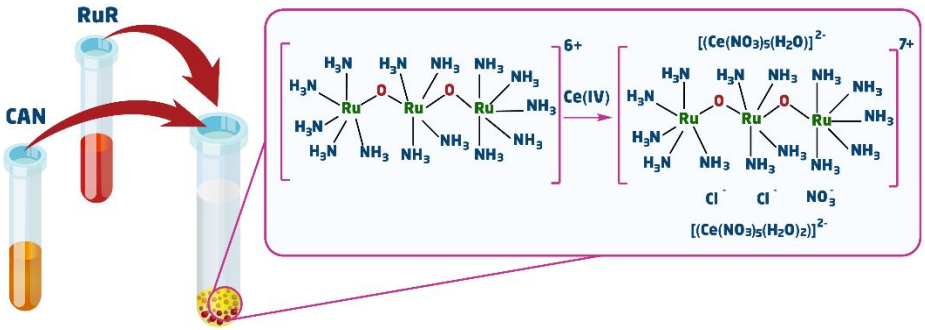


During water-oxidation reaction in the presence of ruthenium red and cerium(IV) ammonium nitrate, a heterogeneous nano-sized ruthenium-cerium compound is detected, which is formed by the electrostatic interaction of $[(NH_3)_5RuORu(NH_3)_4ORu(NH_3)_5]$,$^{6+/7+}$ nitrate ions, and the products of the reduction of cerium(IV) ammonium nitrate.